

A-Site Doped in Perovskite $\text{La}_{(1-x)}\text{Ba}_{x/2}\text{Sr}_{x/2}\text{Mn}_{0.4}\text{Ti}_{0.6}\text{O}_3$ ($x = 0, 0.1, \text{ and } 0.3$) for Absorbing Microwave Material

Sitti Ahmiatri Saptari ^{1,a,*}, Dinda Hapitanur ^{1,b}, Yana Taryana ^{2,c}, Nanang Sudrajat ^{3,d}, Ikhwan Nur Rahman ^{4,e}, and Dwi Nanto ^{5,f}

¹ Department of Physics, UIN Syarif Hidayatullah

Jl. Ir. H. Djuanda No. 95 Ciputat, Kota Tangerang Selatan 15412, Indonesia

² Research Center for Telecommunication, National Research and Innovation Agency

Jl. Cisitua Lama, Dago, Kecamatan Coblong, Kota Bandung 40135, Indonesia

³ Research Center for Advanced Materials, National Research and Innovation Agency
Gedung 224, Jl. Kw. Puspiptek, Muncul, Kec. Setu, Kota Tangerang Selatan 15314, Indonesia

⁴ Department of Physics, Research Institute for Nanoscale and Technology,
Chungbuk National University

Chungdae-ro 1, Seowon-Gu, Cheongju, Chungbuk 28644, Republic of Korea

⁵ Department of Physics Education, UIN Syarif Hidayatullah

Jl. Ir. H. Djuanda No. 95 Ciputat, Kota Tangerang Selatan 15412, Indonesia

e-mail: ^a sitti.ahmiatri@uinjkt.ac.id, ^b dinda.hapitanur18@mhs.uinjkt.ac.id, ^c yana004@brin.go.id,
^d nana017@brin.go.id, ^e ikhwannurrahman@gmail.com, and ^f dwi.nanto@uinjkt.ac.id

* Corresponding Author

Received: 22 July 2023; Revised: 3 November 2023; Accepted: 30 December 2023

Abstract

Microwave radiation can have harmful effects on our bodies. With increased exposure due to online activities, it is essential to use absorber materials like perovskite manganate to reduce radiation. In this study, perovskite manganate $\text{La}_{(1-x)}\text{Ba}_{x/2}\text{Sr}_{x/2}\text{Mn}_{0.4}\text{Ti}_{0.6}\text{O}_3$ ($x = 0, 0.1, \text{ and } 0.3$) was synthesized using the sol-gel method. X-ray diffraction (XRD) analysis revealed that the two samples were multi-phased, LaMnO_3 and $\text{La}_2\text{Ti}_2\text{O}_7$, and were formed, exhibiting a rhombohedral crystal structure ($R\bar{3}c$). Morphological characterization of the sample surface using a Scanning Electron Microscope (SEM) showed that as doping increases, the grain size decreases from 282.02 to 245.63 nm at $x=0$ and $x=0.3$, respectively. This result implies that doping leads to more uniform grain distribution and enhanced grain refinement. Characterization via Vibrating Sample Magnetometer (VSM) revealed that the maximum saturation value, 0.79 emu/g, was attained when $x = 0$. This sample exhibits soft magnetic properties, as evidenced by its coercivity (H_c) value of $< 1\text{ kOe}$. Results from the Vector Network Analyzer (VNA) indicate that the absorption capacity of $\text{La}_{(1-x)}\text{Ba}_{x/2}\text{Sr}_{x/2}\text{Mn}_{0.4}\text{Ti}_{0.6}\text{O}_3$ increases, with a maximum reflection loss value of -25.5 dB with 1.5 mm thickness. Consequently, $\text{La}_{(1-x)}\text{Ba}_{x/2}\text{Sr}_{x/2}\text{Mn}_{0.4}\text{Ti}_{0.6}\text{O}_3$ demonstrates potential as a microwave absorber material.

Keywords: Microwave absorber; perovskite manganate; reflection loss; sol-gel method

How to cite: Saptari S A, et al. A Cite Doped in Perovskite $\text{LaMn}_{0.4}\text{Ti}_{0.6}\text{O}_3$ for Absorbing Electromagnetic Waves Material. *Jurnal Penelitian Fisika dan Aplikasinya (JPFA)*. 2023; 13(2): 106-118.

© 2023 Jurnal Penelitian Fisika dan Aplikasinya (JPFA). This work is licensed under [CC BY-NC 4.0](https://creativecommons.org/licenses/by-nc/4.0/)

INTRODUCTION

The continuous and prolonged use of electronic devices emits electromagnetic wave radiation, which has the potential to adversely affect the functionality of specific organs in the body [1,2]. This concern can be solved by employing electromagnetic wave-absorbing materials. These materials have the capability to transform electromagnetic wave energy into other energy forms, thereby shielding objects from undesired electromagnetic wave exposure [3,4].

Akinay et al. [4] summarize the electromagnetic wave absorber's mechanism by attenuating incoming electromagnetic waves through a combination of reflection, absorption, and transmission at the molecular level. When an electromagnetic wave encounters an absorber material, the incident energy is converted into heat, reducing amplitude. This conversion process can be understood by examining the various interactions between the electromagnetic wave and material interfaces. The absorptive performance of the material is quantified by the reflection loss value, expressed in decibels; a more negative reflection loss signifies better absorption. Dielectric materials exhibit conduction and polarization losses due to ionic, dipole, and interfacial polarization, with the free electron theory explaining the increase in conductivity as a function of the imaginary part of the permittivity.

Furthermore, when considering materials with a magnetic component, the significance of the magnetic loss in the absorption becomes crucial. Magnetic loss results from mechanisms like the eddy current effect and resonance phenomena, including exchange and natural resonance. The absorption efficiency can be elucidated using the energy-component law, which categorizes electromagnetic wave energy into incident, transmitted, and reflected components. This emphasizes the dynamics of energy propagation through the absorber [4].

Extensive research has focused on altering the composition of manganese perovskite to develop an electromagnetic wave absorber material with notable characteristics such as reflectance, particle size, and absorption thickness [5,6]. The architecture of lanthanum manganate, denoted by the chemical formula LaMnO_3 , has been tailored to enhance its magnetic and electrical properties. This improvement is achieved by substituting the La site with 2+ charged alkaline earth ions, such as Ba^{2+} , Sr^{2+} , and Ca^{2+} . These substitutions facilitate a double exchange interaction, causing a transition in the magnetic properties of La-based materials from antiferromagnetic to ferromagnetic. Furthermore, doping the Mn site with transition metal elements can introduce novel electronic states within the bandgap, thereby altering the material's electronic and magnetic properties [7–12].

Nevertheless, this leads to a reduction in magnetic properties due to a diminished Mn^{3+} content. The material's absorptive capability reflects its ability to assimilate electromagnetic waves emitted within specific frequency ranges. Microwave absorption transpires from the wave-material interaction, yielding a reflection loss effect. Reflection loss (RL) quantifies the attenuation caused when electromagnetic waves impinge on a sample. This RL value, representing wave absorption at a specific frequency and thickness, is derived from Vector Network Analyzer (VNA) characterization.

Chen et al. demonstrated that LaTiO_3 exhibits a high dielectric constant when substituted

with Mn at site A [13]. Subsequent research indicated that replacing Ti at site B in LaMnO₃ results in a high dielectric constant [13–15]. Fira et al. synthesized La_{0.7}Ca_{0.3}Mn_{1-x}Ti_xO₃ materials (x = 0, 0.1, 0.2, and 0.3), noting the highest Reflection Loss (RL) value when x = 0.3, registering RL -10.07 dB at a frequency of 10.4 GHz, corresponding to microwave absorption of approximately 90.16% [16]. Li et al. analyzed La_(1-x)Sr_xMnO₃ for x = 0.4 and a thickness of 2.25 mm, identifying an optimal absorption peak around 25 dB [16]. Adi [17] synthesized the material La_(1-y)Ba_yMnO₃ (y = 0-0.7) and reported its ferromagnetic nature, with peak absorption observed when x = 0.2 at a frequency of 14.4 GHz, registering 7 dB. While prior research has involved doping lanthanum with barium and strontium, there remains a gap in the literature concerning using La(Mn, Ti)O₃ as the foundational material and subsequent doping at the La site with both Ba and Sr. In this study, La_(1-x)Ba_{x/2}Sr_{x/2}Mn_{0.4}Ti_{0.6}O₃ (x = 0, 0.1, 0.3) was successfully synthesized via the sol-gel method, examining the dual-doping effects of Sr and Ba incorporation on the crystal structure, morphology, magnetic properties, and, ultimately, microwave-absorbing capabilities.

METHOD

La_(1-x)Ba_{x/2}Sr_{x/2}Mn_{0.4}Ti_{0.6}O₃ samples with x = 0, 0.1, and 0.3 were synthesized using the sol-gel method. The materials used in this study are La₂O₃ (Merck, 99%), Mn(NO₃)₂·4H₂O (Merck, 98.5%), Ba(NO₃)₂ (Merck, 99%), Sr(NO₃)₂ (Merck, 99%), TiO₂ (Merck, 99%) which were then weighed according to the required ratio stoichiometry and dissolved thoroughly with aquadest, except La₂O₃ and TiO₂ must be converted into metal nitrates by reacting them with Nitric acid (HNO₃). All solutions were mixed to form a homogeneous solution and then stirred while heated to a gel-like form. Meanwhile, around ±70 °C, ammonia was added until the solution reached a pH of 7. The next step involved placing the sample at 200 °C for ± 1.5 hours until it transformed into a dry gel to eliminate moisture.

Subsequently, the sample was calcinated in a furnace heated to 600 °C for 6 hours to eliminate organic compound residues and was followed by a sintering process at 1200 °C for 6 hours to enhance crystal bonding and foster crystal formation. The samples were first characterized using X-ray diffraction (XRD) to identify the resultant phase and crystal parameters. The XRD utilized Cu-Kα radiation (λ_{Cu-Kα} = 1.54 Å) and scanned over a 2θ angle range from 10° to 80° in increments of 0.02°. The sample morphology and grain size were then examined using a Scanning Electron Microscope (SEM), operating at a magnification of 20,000x and an accelerating voltage of 20 kV. The material's magnetic properties were ascertained using a Vibrating Sample Magnetometer (VSM) at 297 K, with a magnetic field between 0 and 20,000 Oe. Lastly, a Vector Network Analyzer (VNA) assessed the absorption and RL values of the magnetite powder. The VNA functioned within an 8-12 GHz frequency range with 0.02 GHz increments. Samples were placed in an acrylic holder with dimensions 2.5 cm x 1.5 cm with a 1.5 mm thickness.

RESULTS AND DISCUSSION

XRD characterization revealed that the material La_(1-x)Ba_{x/2}Sr_{x/2}Mn_{0.4}Ti_{0.6}O₃ is multiphasic, as evidenced by impurity peaks. To identify the correct structure crystal, it is used the Goldschmidt tolerance (t_G) [18] formula with doping form as equation (1)

$$t_G = \frac{(1-x)r_{La} + \frac{x}{2}(r_{Ba} + r_{Sr}) + r_O}{\sqrt{2}[0.4r_{Mn} + 0.6r_{Ti} + r_O]}, \quad (1)$$

where r represents the atomic radius. Substituting for x values of 0, 0.1, and 0.3 yielded tG values of 0.95, 0.96, and 0.97, respectively. These values suggest that the incorporation of Ba^{2+} and Sr^{2+} dopants into the $LaMn_{0.4}Ti_{0.6}O_3$ material does not alter the fundamental crystal structure, which retains either an orthorhombic or rhombohedral configuration ($0.9 \leq tG \leq 1$) [19]. Utilizing the COD database [20–23], it matches $LaMnO_3$ (96-153-1527) and $La_2Ti_2O_7$ (96-200-2197) based on peak intensity and position under XRD observations. The X-ray diffraction pattern of the $La_{(1-x)}Ba_{x/2}Sr_{x/2}Mn_{0.4}Ti_{0.6}O_3$ material, depicted in Figure 1(a), exhibits multiphasic characteristics, with the primary phase being $LaMnO_3$ and the secondary phase as $La_2Ti_2O_7$. This observation aligns with the research findings of Pika [14], Wisnu [6], and Hanif [24]. Figures 1(b) and 1(c) illustrate the crystal structures of $LaMn_{0.4}Ti_{0.6}O_3$ and $La_2Ti_2O_7$, respectively. The XRD characterization's diffraction pattern outcomes were subsequently analyzed in greater detail using Rietveld refinement in GSAS-EXPGUI [25], with results summarized in Tables 1 and 2.

Table 1 reveals that substituting Ba and Sr into the $La_{(1-x)}Ba_{x/2}Sr_{x/2}Mn_{0.4}Ti_{0.6}O_3$ material predominantly retains the original crystal structure. However, there is an observed augmentation in the lattice parameters attributable to the doping at the A site, where Ba^{2+} and Sr^{2+} ions occupy the La^{3+} sites. Notably, the ionic radii of Ba^{2+} (1.61 Å) and Sr^{2+} (1.44 Å) exceed that of La^{3+} (1.36 Å). Such A-site doping also amplifies the bond length between Mn and O while diminishing the bond angle. This doping suggests a propensity for the perovskite $LaMnO_3$ to undergo a structural transition towards an orthorhombic configuration. Nevertheless, given the relatively minor value alterations, the overall structure remains unaltered. It is worth noting that such structural transitions can potentially influence the material's thermal properties [26].

The crystallite size was determined using calculations based on the Williamson-Hall method [27], given by the equation (2):

$$\beta \cos \theta = \frac{K\lambda_{Cu}}{D_{W-H}} + 4\varepsilon \sin \theta, \quad (2)$$

where β is the Full Weight Half Maximum (FWHM) of the diffraction peak at position 2θ , ε is strain, $D_{(W-H)}$ is the crystallite size (nm), K is the constant corresponding to the crystal form (0.9), and λ_{Cu} is the wavelength ($Cu = 0.154$ nm).

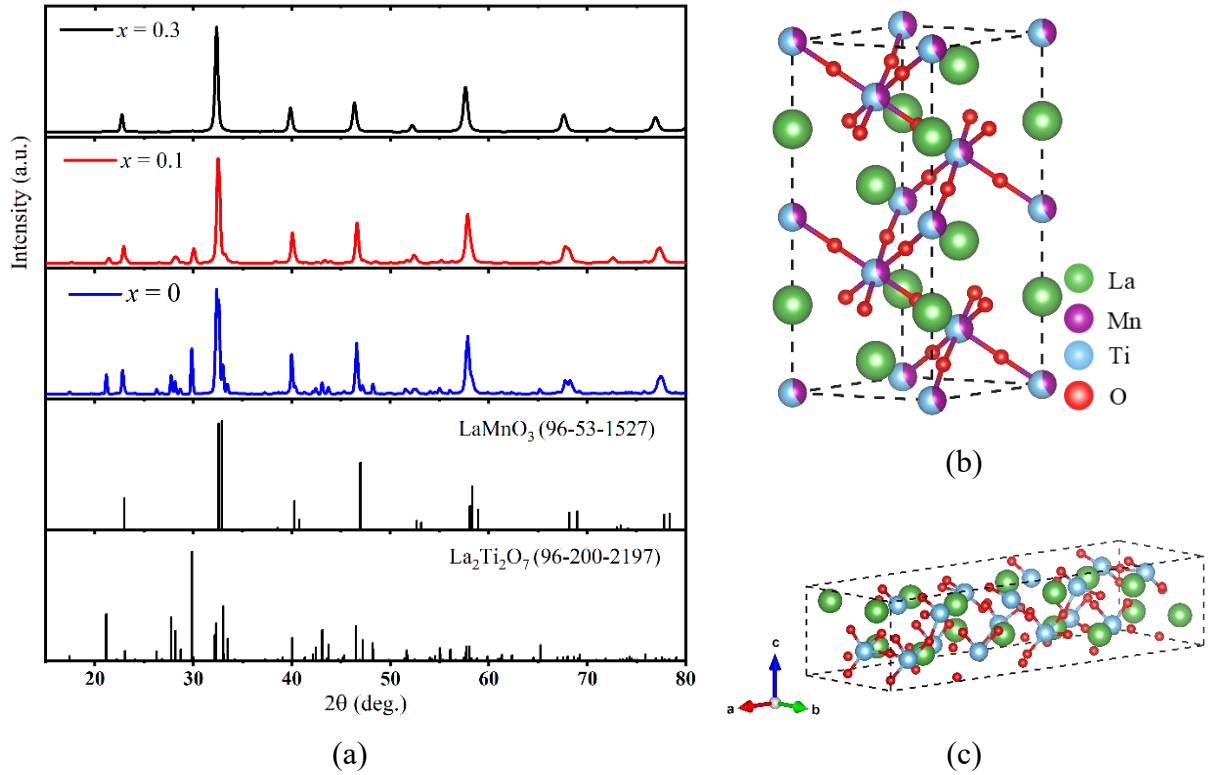


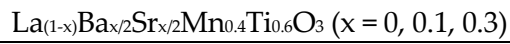
Figure 1. (a) XRD Pattern of $\text{La}_{(1-x)}\text{Ba}_{x/2}\text{Sr}_{x/2}\text{Mn}_{0.4}\text{Ti}_{0.6}\text{O}_3$ ($x = 0, 0.1, 0.3$), (b) Crystal Structure of $\text{LaMn}_{0.4}\text{Ti}_{0.6}\text{O}_3$, and (c) $\text{La}_2\text{Ti}_2\text{O}_7$

Table 1. Structure Parameters of $\text{La}_{(1-x)}\text{Ba}_{x/2}\text{Sr}_{x/2}\text{Mn}_{0.4}\text{Ti}_{0.6}\text{O}_3$ ($x = 0, 0.1, 0.3$)

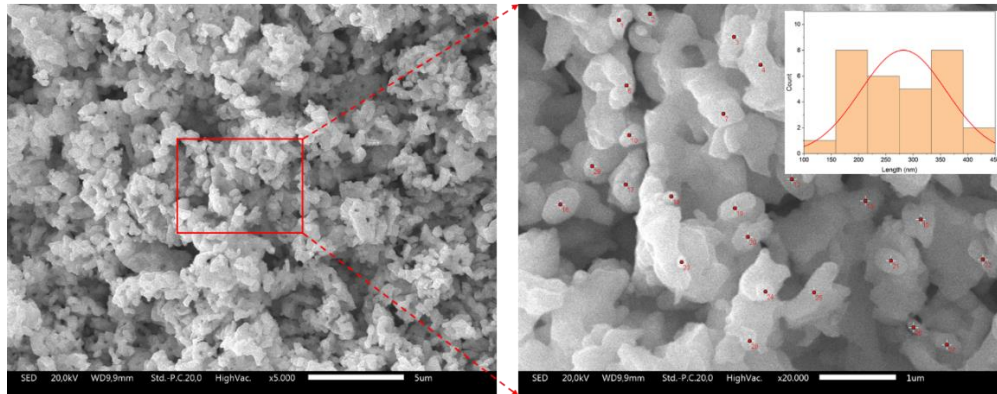
Parameter	$\text{La}_{(1-x)}\text{Ba}_{x/2}\text{Sr}_{x/2}\text{Mn}_{0.4}\text{Ti}_{0.6}\text{O}_3$			$\text{La}_2\text{Ti}_2\text{O}_7$		
	$x = 0$	$x = 0.1$	$x = 0.3$	$x = 0$	$x = 0.1$	$x = 0.3$
Space Group	R -3 c			P n a 21		
Crystal System	Rhombohedral			Orthorhombic		
a (Å)	5.527	5.546	5.544	25.701	25.665	25.786
b (Å)	5.527	5.546	5.544	7.813	7.833	7.806
c (Å)	13.405	13.472	13.579	5.540	5.546	5.682
Volume (Å ³)	354.908	358.817	361.528	1112.638	1114.979	1143.769
Density (g/cm ³)	6.675	6.525	6.330	5.798	5.786	5.378
Weight Fraction (%)	61.084	68.553	98.502	38.916	31.447	1.498
$\langle d_{Mn-O} \rangle$ (Å)	1.95	1.97	1.98			
$\langle \theta_{Mn-O-Mn} \rangle$ (°)	174.6	163.9	161.7			
D_{W-H} (nm)	47.81	92.44	38.52			
ε (%)	0.395	0.205	0.177			

SEM analysis reveals the morphology and grain size of the material, as depicted in Figure 2. Particle shapes are predominantly irregular, with their relatively diminutive sizes attributed to $\text{La}_2\text{Ti}_2\text{O}_7$ impurities. The SEM images were further analyzed using ImageJ2 [28] to measure the average grain size of each sample. It was selected 30 points from each sample and calculated their distribution, with the results in Table 2.

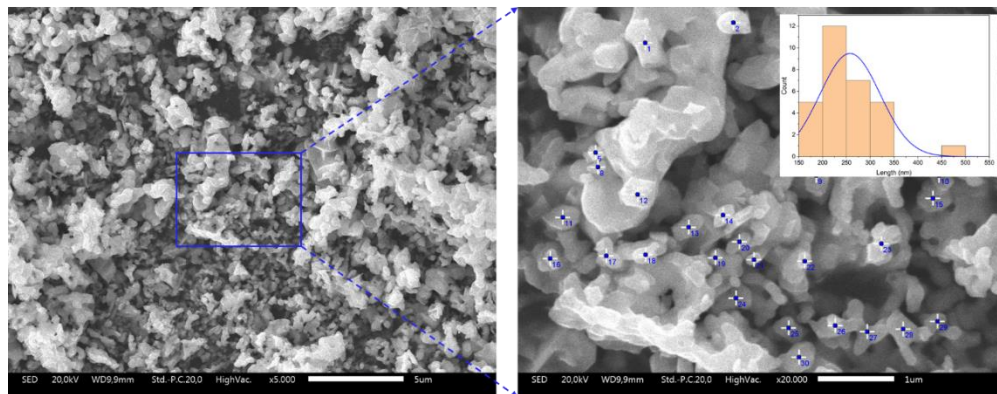
Table 2. Crystallite, Grain Size



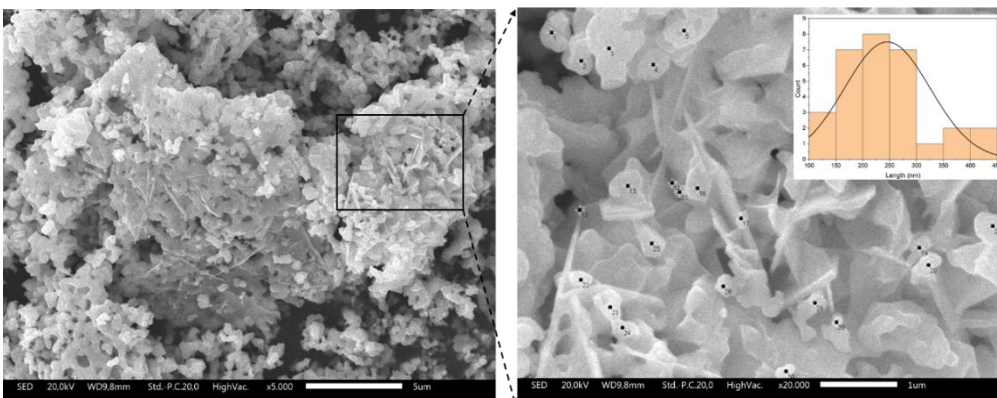
Doping x	Crystallite Size (nm)	Strain (%)	Grain Size (nm)	
			Mean	STD
0	47.81	0.395	282.02	78.57
0.1	92.44	0.205	257.77	63.12
0.3	38.52	0.177	245.63	79.76



(a)



(b)



(c)

Figure 2. Morphological Results of SEM $\text{La}_{(1-x)}\text{Ba}_{x/2}\text{Sr}_{x/2}\text{Mn}_{0.4}\text{Ti}_{0.6}\text{O}_3$ with (a) $x = 0$, (b) $x = 0.1$, and (c) $x = 0.3$

Table 2 illustrates the effects of doping concentration, denoted by 'x', on the crystallite size, strain, and grain size of $\text{La}_{(1-x)}\text{Ba}_{(x/2)}\text{Sr}_{(x/2)}\text{Mn}_{0.4}\text{Ti}_{0.6}\text{O}_3$ perovskite structure. A discernible trend emerges upon increasing the doping concentration. With no doping ($x=0$), the crystallite size is observed to be 47.81 nm, which increases significantly to 92.44 nm for a doping concentration of 0.1. However, further increasing the doping level to 0.3 decreases crystallite size to 38.52 nm. Such non-linear behavior might stem from intricate dopant-lattice interactions, hinting at an optimal doping concentration, seemingly near $x=0.1$, that maximizes the crystallite size. However, more rigorous exploration is essential at escalated doping levels and in producing a single-phase crystal to corroborate this observation. In terms of strain, an inverse relationship with doping concentration is evident. Strain decreases consistently from 0.395% at $x=0$ to 0.177% at $x=0.3$. This decrease suggests that introducing Ba and Sr dopants can effectively relieve lattice strain in the material, enhancing its structural stability.

The grain size exhibits a decreasing trend as doping increases. The average grain size decreases from 282.02 to 245.63 nm at $x=0$ and $x=0.3$, respectively. Concurrently, the standard deviation (STD) values indicate a general decrease in grain size dispersion with increased doping, reaching their lowest at $x=0.1$ before slightly increasing at $x=0.3$. This data implies that doping leads to more uniform grain distribution but with an increase in overall grain refinement. The grain size in polycrystalline materials influences the electron transfer process; smaller grain sizes result in more complex electron transfer, leading to increased resistivity within the material.

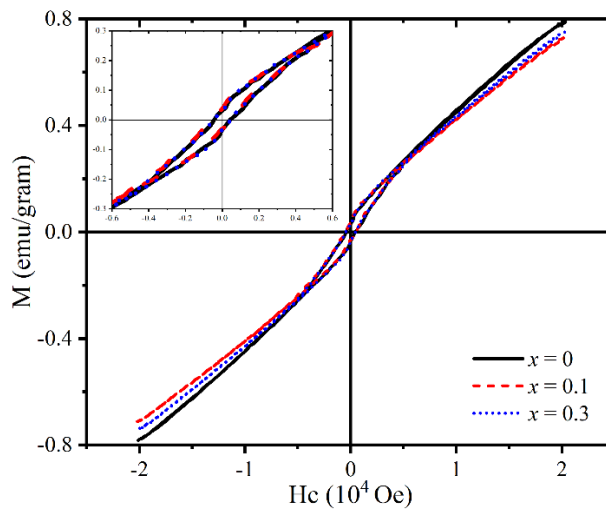


Figure 3. Hysteresis Curve $\text{La}_{(1-x)}\text{Ba}_{x/2}\text{Sr}_{x/2}\text{Mn}_{0.4}\text{Ti}_{0.6}\text{O}_3$

Table 3. Magnetization Parameter Data $\text{La}_{(1-x)}\text{Ba}_{x/2}\text{Sr}_{x/2}\text{Mn}_{0.4}\text{Ti}_{0.6}\text{O}_3$ ($x = 0, 0.1, 0.3$)

Doping x	M_s (emu/g)	M_r (emu/g)	H_c (Oe)
0	0.79	0.03	434.15
0.1	0.73	0.04	497.00
0.3	0.75	0.03	463.07

Analysis of the hysteresis curve depicted in Figure 3 suggests a magnetic phase transformation, underscored by the material's saturation, remanence, and coercivity values

detailed in Table 3. As evident from Table 3, the $\text{La}_{(1-x)}\text{Ba}_{x/2}\text{Sr}_{x/2}\text{Mn}_{0.4}\text{Ti}_{0.6}\text{O}_3$ material can be classified as a soft magnet due to its coercivity value being less than 1 kOe. In the range $x = 0$ to 0.1, the material's permeability diminishes upon introducing Ba and Sr, manifested as a reduction in the saturation field. As posited by Yadav et al. and Navin et al., a decrease in crystallite size correlates with a reduction in magnetic saturation. This phenomenon is attributed to lattice irregularities, especially structural relaxation, which significantly drive magnetic changes in such fine particles [29–31].

However, when $x = 0.3$, there is an observed increase in permeability, evidenced by the heightened value of the saturation field compared to $x = 0.1$. As suggested by Orgiani et al., doping can modify the electronic structure of a material, which subsequently impacts its double-exchange interactions and, by extension, its magnetic properties [32]. In this case, the fluctuations in permeability can be attributed to disruptions in the double-exchange interaction between Mn^{3+} and Mn^{4+} . Additionally, the X-ray diffraction patterns indicate that the structures for compositions $x = 0$ and 0.1 contain a more substantial proportion of impurity $\text{La}_2\text{Ti}_2\text{O}_7$. Research by Amor et al. and Jacko et al. has demonstrated that $\text{La}_2\text{Ti}_2\text{O}_7$ phases are non-magnetic, leading to diminished permeability values [33,34].

The investigation results from the VNA reveal a Reflection Loss (RL) curve for microwaves within the X-band frequency range (8-12 GHz). Figure 4 displays a singular absorption point, calculated using the Through Power formula presented in equation (3), where Γ represents the reflection coefficient and is given by $\Gamma = 10^{\text{RL}/20}$.

$$\text{Through Power (\%)} = 100 \times (1 - |\Gamma|^2) \tag{3}$$

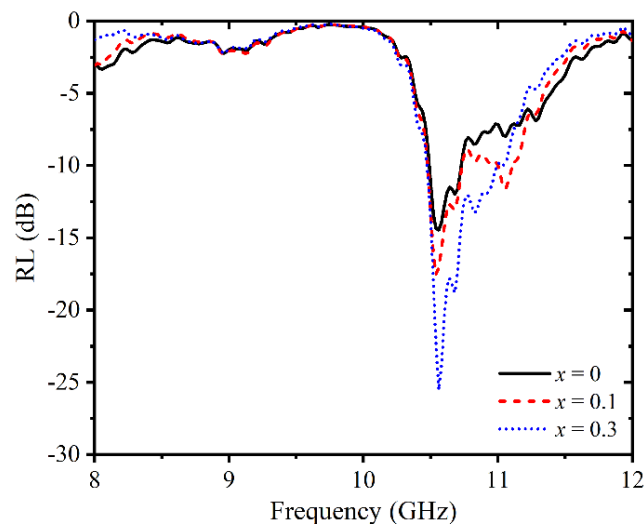


Figure 3. Graph of the Combined Relationship of Reflection Loss with the Frequency of $\text{La}_{(1-x)}\text{Ba}_{x/2}\text{Sr}_{x/2}\text{Mn}_{0.4}\text{Ti}_{0.6}\text{O}_3$

Based on Table 4, the absorption capability of $\text{La}_{(1-x)}\text{Ba}_{x/2}\text{Sr}_{x/2}\text{Mn}_{0.4}\text{Ti}_{0.6}\text{O}_3$ appears to enhance with increasing Ba and Sr dopant composition. The peak RL value reaches -25.5 dB at an optimal frequency of 10.56 GHz for $x = 0.3$. Additionally, the VNA's analysis of physical properties yielded reactance and resistance values, which were subsequently used to derive impedance and reflection loss values. The most pronounced negative reflection loss is achieved when the resistance approaches 50Ω , coupled with minimal reactance.

Table 4. VNA Characterization Results at Maximum Reflection Loss of $\text{La}_{(1-x)}\text{Ba}_x/2\text{Sr}_x/2\text{Mn}_{0.4}\text{Ti}_{0.6}\text{O}_3$ ($x = 0, 0.1, 0.3$)

Parameters	$\text{La}_{(1-x)}\text{Ba}_x/2\text{Sr}_x/2\text{Mn}_{0.4}\text{Ti}_{0.6}\text{O}_3$		
	$x = 0$	$x = 0.1$	$x = 0.3$
Frequency (GHz)	10.56	10.54	10.56
Reflection Loss (dB)	-14.5	-17.5	-25.5
Resistance (Ω)	34.641	38.372	45.020
Reactance (Ω)	4.674	1.675	0.688
Z	$34.641 + i 4.674$	$38.372 + i 1.675$	$45.020 + i 0.688$
$ \Gamma $	0.189	0.133	0.053
Through Power (%)	96.45	98.22	99.72

The diverse results presented raise several concerns. One relates to the phases formed during synthesis, as evidenced by XRD characterization, and the consistency in particle size as depicted by SEM imaging. Creating materials with a singular phase and a consistent, small grain size is vital. Such a strategy ensures that the properties of the sample under investigation remain unadulterated by external factors or contaminants. Among the three sample types ($x = 0, 0.1,$ and 0.3), only $x = 0.3$ showcases a singular phase marked by a superior RF value compared to its counterparts. Conversely, $x = 0.1$ exhibits crystal and particle size variations relative to the others. While several studies employing the same synthesis method report the existence of similar impurities [6,14,15,24], the VNA data compellingly highlights the influence of x doping.

Table 5. Comparative Analysis of Reflection Loss in Various Manganate Perovskite Materials

Material	Thickness (mm)	Frequency (GHz)	Reflection Loss (dB)	References
$\text{LaMn}_{0.4}\text{Ti}_{0.6}\text{O}_3$	1.5	10.56	-14.50	This work
$\text{La}_{0.9}\text{Ba}_{0.05}\text{Sr}_{0.05}\text{Mn}_{0.4}\text{Ti}_{0.6}\text{O}_3$	1.5	10.54	-17.50	This work
$\text{La}_{0.7}\text{Ba}_{0.15}\text{Sr}_{0.15}\text{Mn}_{0.4}\text{Ti}_{0.6}\text{O}_3$	1.5	10.56	-25.50	This work
$\text{La}_{0.8}\text{Ba}_{0.2}\text{Mn}_{0.8}\text{Fe}_{0.1}\text{Ti}_{0.1}\text{O}_3$	1.5	10.5	-24.00	[35]
$\text{La}_{0.6}\text{Sr}_{0.4}\text{MnO}_3$	2.25	9.5	-25.00	[36]
$\text{La}_{0.7}\text{Ca}_{0.3}\text{Mn}_{0.7}\text{Ti}_{0.3}\text{O}_3$	1.5	10.4	-10.07	[15]
$\text{La}_{0.7}\text{Ca}_{0.3}\text{MnO}_3$	1.5	10.44	-3.53	[37]
$\text{La}_{0.7}(\text{Ca}_{0.9}\text{Sr}_{0.1})_{0.3}\text{MnO}_3$	1.5	10.42	-3.11	[37]

Table 5 highlights reflection loss values for distinct perovskite materials. The primary compound under consideration, $\text{La}_{0.7}\text{Ba}_{0.15}\text{Sr}_{0.15}\text{Mn}_{0.4}\text{Ti}_{0.6}\text{O}_3$, registers an impressive -25.50 dB at 10.56 GHz. This result indicates the compound's potential as an effective electromagnetic wave absorber. Nonetheless, comprehensive engineering considerations, including design and development, are essential to transition this material into a functional electromagnetic absorber device. With innovative strategies and methodologies, there is an opportunity to refine the material's attributes, paving the way for a more practical solution in real-world electromagnetic absorption scenarios.

Nevertheless, Further research is essential to produce $\text{La}_{(1-x)}\text{Ba}_x/2\text{Sr}_x/2\text{Mn}_{0.4}\text{Ti}_{0.6}\text{O}_3$ samples consistently exhibiting a singular phase for each x variation, including at elevated x values. This endeavor might benefit from implementing a different synthesis approach [38].

CONCLUSION

$\text{La}_{(1-x)}\text{Ba}_{x/2}\text{Sr}_{x/2}\text{Mn}_{0.4}\text{Ti}_{0.6}\text{O}_3$ was successfully synthesized with compositions of $x = 0, 0.1,$ and 0.3 using the sol-gel method. XRD analysis revealed a rhombohedral structure (R-3c) in the sample, with an increase in the primary phase composition as the value of x increased. The substitution of Ba^{2+} and Sr^{2+} ions did not alter the structure but changed the lattice parameters, volume, and crystallite size. Morphological characterization of the sample surface showed that as doping increases, the grain size decreases from 282.02 nm to 245.63 nm at $x=0$ and $x=0.3$, respectively. This result implies that doping leads to more uniform grain distribution and enhanced grain refinement. VSM analysis showed that doping Ba and Sr at the La site decreased magnetic properties; however, when $x = 0.3$, there was an increase in the saturation value relative to when $x = 0.1$. This material exhibits soft magnetic properties, as evidenced by a coercivity value (H_c) of < 1 kOe. VNA characterization indicated that the highest reflection loss value, with an RL of -25.5 dB at an optimal frequency of 10.56 GHz, was achieved when $x = 0.3$. Consequently, $\text{La}_{(1-x)}\text{Ba}_{x/2}\text{Sr}_{x/2}\text{Mn}_{0.4}\text{Ti}_{0.6}\text{O}_3$ shows potential as a microwave absorber material.

ACKNOWLEDGMENT

This research was partially funded by a grant from UIN Syarif Hidayatullah Jakarta UN.01/KPA/223/2022 and the national research and innovation agency.

AUTHOR CONTRIBUTIONS

Sitti Ahmiatri Saptari: Conceptualization, Methodology, Visualization, Writing - Original Draft, Resources, Supervision; Dinda Hapitanur: Formal Analysis, Methodology, Investigation, Writing - Original Draft; Yana Taryana: Investigation, Resources; Nanang Sudrajat: Investigation; Ikhwan Nur Rahman: Formal Analysis, Methodology; and Dwi Nanto: Writing - Review & Editing, Visualization.

DECLARATION OF COMPETING INTEREST

The authors declare that they have no known competing financial interests or personal relationships that could have appeared to influence the work reported in this paper.

REFERENCES

- [1] Hu C, Zuo H, and Li Y. Effects of Radiofrequency Electromagnetic Radiation on Neurotransmitters in the Brain. *Front Public Health*. 2021; **9**: 691880. DOI: <https://doi.org/10.3389/fpubh.2021.691880>.
- [2] Liu X, Yan X, Zhang S, Liu Z, Win TTY, and Ren L. The Effects of Electromagnetic Fields on Human Health: Recent Advances and Future. *Journal of Bionic Engineering*. 2021; **18**: 210–237. DOI: <https://doi.org/10.1007/s42235-021-0015-1>.
- [3] Taryana Y, Manaf A, Sudrajat N, and Wahyu Y. Electromagnetic Wave Absorbing Materials on Radar Frequency Range. *Jurnal Keramik dan Gelas Indonesia*. 2019; **28**(1): 1-28. DOI: <https://doi.org/10.32537/jkgi.v28i1.5197>.
- [4] Akinay Y, Gunes U, Çolak B, and Cetin T. Recent Progress of Electromagnetic Wave Absorbers: A Systematic Review and Bibliometric Approach. *ChemPhysMater*. 2023; **2**(3): 197-206. DOI: <https://doi.org/10.1016/j.chphma.2022.10.002>.
- [5] Aritonang S, Adi WA, Juhana R, and Herawan T. Structural and Reflection Loss Properties of Fe^{3+} Substituted Lanthanum Manganite as Microwave Absorbing Material in X-ku Band.

- In Chaari F, Gherardini F, Ivanov V, and Haddar M (Eds.), *Lecture Notes in Mechanical Engineering*. Singapore: Springer Singapore; 2021: 949–959. DOI: https://doi.org/10.1007/978-981-15-9505-9_83.
- [6] Adi WA, Sarwanto Y, Taryana Y, and Soegijono B. Effects of The Geometry Factor on The Reflection Loss Characteristics of The Modified Lanthanum Manganite. *Journal of Physics: Conference Series*. 2018; **1091**: 012028. DOI: <https://doi.org/10.1088/1742-6596/1091/1/012028>.
- [7] Rahmouni H, Dhahri A, and Khirouni K. The effect of Tin Addition on The Electrical Conductivity of Sn-doped LaBaMnO₃. *Journal of Alloys and Compound*. 2014; **591**: 259–262. DOI: <https://doi.org/10.1016/j.jallcom.2013.12.108>.
- [8] Moratal S, Benavente R, Salvador MD, Peñaranda-Foix FL, Moreno R, and Borrell A. Microwave Sintering Study of Strontium-Doped Lanthanum Manganite in A Single-Mode Microwave with Electric and Magnetic Field at 2.45 GHz. *Journal of The European Ceramic Society*. 2022; **42**: 5624–5630. DOI: <https://doi.org/10.1016/j.jeurceramsoc.2022.05.060>.
- [9] Lee YH and Mahendiran R. Transport and Electron Spin Resonance Studies in Mo-doped LaMnO₃. *AIP Advances*. 2023; **13**(2): 025115. DOI: <https://doi.org/10.1063/9.0000442>.
- [10] Mo H, Nan H, Lang X, Liu S, Qiao L, Hu X, and Tian H. Influence Of Calcium Doping on Performance of LaMnO₃ Supercapacitors. *Ceramics International*. 2018; **44**(8): 9733–9741. DOI: <https://doi.org/10.1016/j.ceramint.2018.02.205>.
- [11] Vazhayil A, Thomas J, and Thomas N. Cobalt Doping in LaMnO₃ Perovskite Catalysts – B Site Optimization by Solution Combustion for Oxygen Evolution Reaction. *Journal of Electroanalytical Chemistry*. 2022; **918**: 116426. DOI: <https://doi.org/10.1016/j.jelechem.2022.116426>.
- [12] Autieri C, Cuoco M, Cuono G, Picozzi S, and Noce C. Orbital Order and Ferromagnetism in LaMn_{1-x}Ga_xO₃. *Physica B Condens Matter*. 2023; **648**: 414407. DOI: <https://doi.org/10.1016/j.physb.2022.414407>.
- [13] Chen Y, Yan QQ, and Cui YM. Dielectric Properties of A, B-Site Mn-Doped LaTiO_{3+δ}. *Materials Science Forum*. 2018; **921**: 78–84. DOI: <https://doi.org/10.4028/www.scientific.net/MSF.921.78>.
- [14] Jha P, Rai S, Ramanujachary KV, Lofland SE, and Ganguli AK. (La_{0.4}Ba_{0.4}Ca_{0.2})(Mn_{0.4}Ti_{0.6})O₃: A New Titano-Manganate With A High Dielectric Constant and Antiferromagnetic Interactions. *Journal of Solid State Chemistry*. 2004; **177**(8): 2881–2888. DOI: <https://doi.org/10.1016/j.jssc.2004.05.009>.
- [15] Rizky F, Saptari SA, Tjahjono A, and Khaerudini DS. Perovskite Manganit Analysis Based on La_{0.7}Ca_{0.3}Mn_{1-x}Ti_xO₃ (x=0, 0.1, 0.2, and 0.3) as Potential Microwave Absorber Material with Sol-Gel Method. *Journal of Physics: Theories and Application*. 2022; **6**(1): 17-24. DOI: <https://doi.org/10.20961/jphystheor-appl.v6i1.59142>.
- [16] Li G, Hu G-G, Zhou H-D, Fan X-J, and Li X-G. Absorption of Microwaves in La_{1-x}Sr_xMnO₃ Manganese Powders Over A Wide Bandwidth. *Journal of Applied Physics*. 2001; **90**(11): 5512–5514. DOI: <https://doi.org/10.1063/1.1415053>.
- [17] Adi WA. *Pengembangan Bahan Magnetik Sistem La_(1-Y)Ba_YFe_xMn_{½(1-X)}Ti_{½(1-X)}O₃ (X = 0 – 1,0 Dan Y = 0 – 1,0) Sebagai Bahan Penyerap Gelombang Elektromagnetik*. Dissertation. Depok: Universitas Indonesia; 2014.
- [18] Goldschmidt VM. Die Gesetze der Krystallochemie. *Naturwissenschaften*. 1926; **14**: 477–485. DOI: <https://doi.org/10.1007/BF01507527>.

- [19] Behara S and Thomas T. Stability and Amphotericity Analysis in Rhombohedral ABO₃ Perovskites. *Materialia*. 2020; 13: 100819. DOI: <https://doi.org/10.1016/j.mtla.2020.100819>.
- [20] Vaitkus A, Merkys A, and Gražulis S. Validation of the Crystallography Open Database using the Crystallographic Information Framework. *Journal of Applied Crystallography*. 2021; 54: 661–672. DOI: <https://doi.org/10.1107/S1600576720016532>.
- [21] Gražulis S, Daškevič A, Merkys A, Chateigner D, Lutterotti L, Quirós M, et al. Crystallography Open Database (COD): An Open-Access Collection of Crystal Structures and Platform for World-Wide Collaboration. *Nucleic Acids Research*. 2012; 40(D1): D420–D427. DOI: <https://doi.org/10.1093/nar/gkr900>.
- [22] Gražulis S, Chateigner D, Downs RT, Yokochi AFT, Quirós M, Lutterotti L, et al. Crystallography Open Database – An Open-Access Collection of Crystal Structures. *Journal of Applied Crystallography*. 2009; 42: 726–729. DOI: <https://doi.org/10.1107/S0021889809016690>.
- [23] Merkys A, Vaitkus A, Grybauskas A, Konovalovas A, Quirós M, and Gražulis S. Graph Isomorphism-Based Algorithm for Cross-Checking Chemical and Crystallographic Descriptions. *Journal of Cheminformatics*. 2023; 15: 25. DOI: <https://doi.org/10.1186/s13321-023-00692-1>.
- [24] Hanif SH bt M, Primus WC, and Sinin AE. Effect of Strontium Doping on Structural and Electrical Properties of LMTO Ceramic. *AIP Conference Proceedings*. 2021; 2332(1): 040003. DOI: <https://doi.org/10.1063/5.0042872>.
- [25] Toby BH. EXPGUI, A Graphical User Interface for GSAS. *Journal of Applied Crystallography*. 2001; 34: 210–213. DOI: <https://doi.org/10.1107/S0021889801002242>.
- [26] Qu X-Y, Gou X-F, and Wang T-G. A Highly Accurate Interatomic Potential for LaMnO₃ Perovskites with Temperature-Dependence of Structure and Thermal Properties. *Computational Materials Science*. 2021; 193: 110406. DOI: <https://doi.org/10.1016/j.commatsci.2021.110406>.
- [27] Hamdi R, Hayek SS, Samara A, Tong Y, Mansour SA, and Haik Y. Williamson-Hall Technique for Magnetic Cooling in Nanosized Manganite LaNi_{0.25}Mn_{0.75}O₃ and Ferrite LaNi_{0.25}Fe_{0.75}O₃. *Solid State Sciences*. 2023; 142: 107223. DOI: <https://doi.org/10.1016/j.solidstatesciences.2023.107223>.
- [28] Rueden CT, Schindelin J, Hiner MC, DeZonia BE, Walter AE, Arena ET, and Eliceiri KW. ImageJ2: ImageJ for The Next Generation of Scientific Image Data. *BMC Bioinformatics*. 2017; 18: 529. DOI: <https://doi.org/10.1186/s12859-017-1934-z>.
- [29] Yadav PA, Deshmukh A V, Adhi KP, Kale BB, Basavaiah N, and Patil SI. Role of Grain Size on The Magnetic Properties of La_{0.7}Sr_{0.3}MnO₃. *Journal of Magnetism and Magnetic Materials*. 2013; 328: 86–90. DOI: <https://doi.org/10.1016/j.jmmm.2012.09.056>.
- [30] Navin K and Kurchania R. The Effect of Particle Size on Structural, Magnetic and Transport Properties of La_{0.7}Sr_{0.3}MnO₃ Nanoparticles. *Ceramics International*. 2018; 44(5): 4973–4980. DOI: <https://doi.org/10.1016/j.ceramint.2017.12.091>.
- [31] Navin K and Kurchania R. The Effect of Shell Layer on Magnetic, Transport, and Electrochemical Properties of La_{0.7}Sr_{0.3}MnO₃ Nanoparticles. *Ceramics International*. 2021; 47(11): 15859–15867. DOI: <https://doi.org/10.1016/j.ceramint.2021.02.160>.
- [32] Orgiani P, Galdi A, Aruta C, Cataudella V, De Filippis G, Perroni CA, et al. Multiple Double-Exchange Mechanism by Mn²⁺ Doping in Manganite Compounds. *Physics Review B*. 2010; 82: 205122. DOI: <https://doi.org/10.1103/PhysRevB.82.205122>.

- [33] Amor N Ben, Bejar M, Dhahri E, Bekri M, Valente MA, and Hlil EK. Study of the Physical Properties of $\text{La}_{2-x}\text{Er}_x\text{Ti}_2\text{O}_7$ ($0 \leq x \leq 0.075$) Compounds. *The European Physical Journal Applied Physics*. 2012; **59**: 10601. DOI: <https://doi.org/10.1051/epjap/2012120142>.
- [34] Jacko R, Csach K, Pristáš G, Mihalik Jr. M, Zentková M, and Mihalik M. Magnetic Properties of $(\text{Dy}_x\text{La}_{1-x})_2\text{Ti}_2\text{O}_7$. *Acta Physica Polonica A*. 2020; **137**: 997–999. DOI: <https://doi.org/10.12693/APhysPolA.137.997>.
- [35] Adi WA, Indro MN, and Kusumastuti AA. Effect of Manganese Addition on the Structure, Magnetic Properties and Microwave Absorption of $\text{La}_{0.8}\text{Ba}_{0.2}\text{Mn}_x\text{Fe}_{\frac{1}{2}(1-x)}\text{Ti}_{\frac{1}{2}(1-x)}\text{O}_3$. *IOP Conference Series: Earth and Environmental Science*. 2017; **58**: 012047. DOI: <https://doi.org/10.1088/1755-1315/58/1/012047>.
- [36] Li G, Hu G-G, Zhou H-D, Fan X-J, and Li X-G. Attractive Microwave-Absorbing Properties of $\text{La}_{1-x}\text{Sr}_x\text{MnO}_3$ Manganite Powders. *Materials Chemistry and Physics*. 2002; **75**(1-3): 101–104. DOI: [https://doi.org/10.1016/S0254-0584\(02\)00039-1](https://doi.org/10.1016/S0254-0584(02)00039-1).
- [37] Admi RI, Saptari SA, Tjahjono A, Rahman IN, and Adi WA. Synthesis and Characterization Microwave Absorber Properties of $\text{La}_{0.7}(\text{Ca}_{1-x}\text{Sr}_x)_{0.3}\text{MnO}_3$ Prepared by Sol-Gel Method. *Journal of Physics: Conference Series*. 2021; **1816**: 012091. DOI: <https://doi.org/10.1088/1742-6596/1816/1/012091>.
- [38] Kumar D, Yadav RS, Monika, Singh AK, and Rai SB. Synthesis Techniques and Applications of Perovskite Materials. In Tian H. *Perovskite Materials, Devices and Integration*. London: IntechOpen; 2020. DOI: <https://doi.org/10.5772/intechopen.86794>.